

HOW TO CITE:

Nel AE, Morschhauser A, Vervelidou F, Matzka J. A new high-resolution geomagnetic field model for southern Africa [supplementary material]. S Afr J Sci. 2024;120(1/2), Art. #11809.

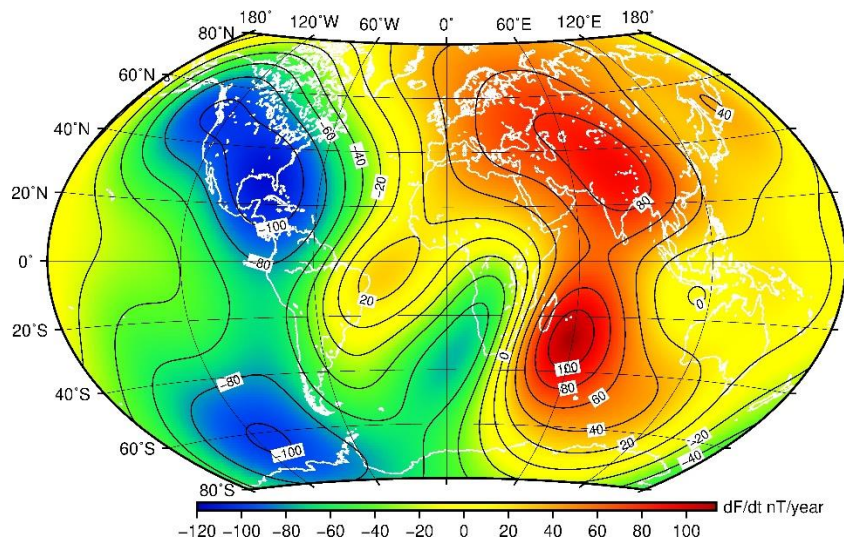
<https://doi.org/10.17159/sajs.2024/11809/suppl>

Supplementary table 1: Total field values in nanoTesla of the repeat stations for all available years (F15–F18) and the secular variation in nanoTesla/year derived from those values (SV1516–SV1718). The yellow highlighted rows show data recorded and collected on the west leg, and the blue highlighted rows show data recorded and collected on the east leg. The average value for each respective secular variation is indicated by AVG W and AVG E.

LAT [degrees]	LON [degrees]	F15 [nT]	F16 [nT]	F17 [nT]	F18 [nT]	SV1516 [nT/year]	SV1617 [nT/year]	SV1718 [nT/year]	
-30.05	19.47	26274	26245	26195	26121	-30	-51	-74	
-32.17	25.63	26933	26920	26894	26872	-14	-26	-22	
-30.95	23.15	26517	26493	26456	26414	-24	-38	-43	
-30.6	17.98	26081	26021	25957	25881	-61	-64	-76	
-34.02	22.37	26064	26037	26007	25959	-27	-30	-48	
-34.02	24.78	26444	26422	26390	26371	-23	-33	-20	
-32.78	20.53	26051	26026	25980	25922	-25	-47	-58	
-29.22	27.47	27515	27509	27484	27474	-6	-26	-11	
-22.37	30.03	29427	29407	29396	29390	-21	-11	-7	
-27.08	30.88	28523	28526	28522	28522	4	-5	-1	
-28.35	32.43	28774	28790	28791	28809	17	1	19	
-26.58	22.85	27680	27598	27557	27502	-82	-42	-55	
-29.78	29.48	27895	27910	27890	27892	15	-20	2	
-28.42	21.3	27255	27176	27125	27060	-79	-52	-65	
-31.35	20.93	26345	26265	26219	26160	-80	-46	-59	
						AVG W	-47	-50	-55
						AVG E	-1	-14	-3

Supplementary table 2: The same locations for the repeat stations were used to derive the Total Field and Secular Variation using the CHAOS model. The average value of the Secular Variation is shown in the rows titled AVG W and AVG E, corresponding to locations on the west leg and east leg, respectively.

LAT [degrees]	LON [degrees]	F15 [nT]	F16 [nT]	F17 [nT]	F18 [nT]	SV1516 [nT/year]	SV1617 [nT/year]	SV1718 [nT/year]
-30.05	19.47	19736	19715	19692	19669	-22	-24	-23
-32.17	25.63	20735	20725	20714	20703	-11	-12	-11
-30.95	23.15	19057	19044	19030	19016	-14	-15	-14
-30.6	17.98	24317	24272	24226	24179	-45	-47	-47
-34.02	22.37	24805	24776	24746	24717	-29	-31	-29
-34.02	24.78	24989	24970	24950	24933	-19	-20	-18
-32.78	20.53	20748	20727	20703	20681	-22	-24	-23
-29.22	27.47	14906	14902	14897	14893	-4	-5	-5
-22.37	30.03	24711	24703	24693	24685	-8	-10	-9
-27.08	30.88	18666	18665	18663	18661	-2	-3	-2
-28.35	32.43	28704	28717	28728	28742	13	12	15
-26.58	22.85	19413	19398	19380	19364	-16	-18	-17
-29.78	29.48	16994	16992	16989	16986	-3	-4	-3
-28.42	21.3	20953	20932	20908	20885	-22	-24	-24
-31.35	20.93	18765	18749	18731	18714	-17	-18	-18
AVG W						-23	-25	-24
AVG E						-3	-4	-3



Source: Image reproduced with permission of the British Geological Survey ©UKRI 2023.¹

Supplementary figure 1: Map of the annual rate of change of total field intensity from IGRF-13, given in dF/df nT/year, for 2020–2025.²

References

1. British Geological Survey. International Geomagnetic Reference Field (IGRF) [webpage on the Internet]. c2019 [cited 2023 Nov 10]. Available from: <https://geomag.bgs.ac.uk/research/modelling/IGRF.html>
2. Alken P, Thébault E, Beggan CD, Amit H, Aubert J, Baerenzung J, et al. International Geomagnetic Reference Field: The thirteenth generation. *Earth Planets Space*. 2021;73, Art. #49. <https://doi.org/10.1186/s40623-020-01288-x>